Nanoscale

PAPER

View Article Online
View Journal | View Issue

Cite this: *Nanoscale*, 2016, **8**, 3386

Magnetically actuated tissue engineered scaffold: insights into mechanism of physical stimulation

Yulia Sapir-Lekhovitser,[a] Menahem Y. Rotenberg,[a] Juergen Jopp,[b] Gary Friedman,[c,d] Boris Polyak*[c,e] and Smadar Cohen*[a,b,f]

Providing the right stimulatory conditions resulting in efficient tissue promoting microenvironment *in vitro* and *in vivo* is one of the ultimate goals in tissue development for regenerative medicine. It has been shown that in addition to molecular signals (*e.g.* growth factors) physical cues are also required for generation of functional cell constructs. These cues are particularly relevant to engineering of biological tissues, within which mechanical stress activates mechano-sensitive receptors, initiating biochemical pathways which lead to the production of functionally mature tissue. Uniform magnetic fields coupled with magnetizable nanoparticles embedded within three dimensional (3D) scaffold structures remotely create transient physical forces that can be transferrable to cells present in close proximity to the nanoparticles. This study investigated the hypothesis that magnetically responsive alginate scaffold can undergo reversible shape deformation due to alignment of scaffold's walls in a uniform magnetic field. Using custom made Helmholtz coil setup adapted to an Atomic Force Microscope we monitored changes in matrix dimensions *in situ* as a function of applied magnetic field, concentration of magnetic particles within the scaffold wall structure and rigidity of the matrix. Our results show that magnetically responsive scaffolds exposed to an externally applied time-varying uniform magnetic field undergo a reversible shape deformation. This indicates on possibility of generating bending/stretching forces that may exert a mechanical effect on cells due to alternating pattern of scaffold wall alignment and relaxation. We suggest that the matrix structure deformation is produced by immobilized magnetic nanoparticles within the matrix walls resulting in a collective alignment of scaffold walls upon magnetization. The estimated mechanical force that can be imparted on cells grown on the scaffold wall at experimental conditions is in the order of 1 pN, which correlates well with reported threshold to induce mechanotransduction effects on cellular level. This work is our next step in understanding of how to accurately create proper stimulatory microenvironment for promotion of cellular organization to form mature tissue engineered constructs.

Received 13th August 2015,
Accepted 10th January 2016

DOI: 10.1039/c5nr05500h

www.rsc.org/nanoscale

Introduction

Externally-controlled drug delivery and remote control of cellular behavior for therapeutic and tissue engineering purposes are important clinical areas in which polymeric composite materials have the potential to make significant advances. The homogeneous dispersion of nanometer-scale inorganic species in a polymeric matrix is of great interest, as the polymeric material may gain useful optical, rheological, mechanical, electrical or magnetic properties.[1–5] Magnetic-responsive materials are of a considerable interest because properties of these materials can be controlled in a remote fashion enabling non-invasive (noncontact) forms of actuation.[6]

Colloidal suspensions of magneto-responsive particles dispersed in a carrier medium are often referred to as magnetorheological (MR) fluids.[7] When MR fluids containing superparamagnetic particles are exposed to a magnetic field, the dipole moment induced in the particles causes them to form chains or aggregates. The field-governed structures restrict the free movement of dispersed particles in MR suspensions, thereby inducing significant variations in their

[a]*The Avram and Stella Goldstein-Goren Department of Biotechnology Engineering, Ben-Gurion University of the Negev, Beer-Sheva 84105, Israel. E-mail: scohen@bgu.ac.il*
[b]*Ilse Katz Institute for Nanoscale Science and Technology, Ben-Gurion University of the Negev, Beer-Sheva 84105, Israel*
[c]*Department of Surgery, Drexel University College of Medicine, Philadelphia, PA 19102, USA. E-mail: bpolyak@drexelmed.edu*
[d]*Department of Electrical and Computer Engineering, Drexel University, Philadelphia, PA 19104, USA*
[e]*Department of Pharmacology and Physiology, Drexel University, Philadelphia, PA 19102, USA*
[f]*Center for Regenerative Medicine and Stem Cell (RMSC) Research, Ben-Gurion University of the Negev, Beer-Sheva 84105, Israel*

rheological and viscoelastic properties.[8,9] In contrast to colloidal dispersions, magnetic nanoparticles embedded in solid or semi-solid (*e.g.* hydrogels) materials are assumed to be locked in place possessing little mechanical freedom. In this case, the semi-solid material is expected to respond as an entire structure, changing its 3D alignment, porosity and dimensions.

The ability to remotely control properties of materials and consequently the behavior of biological objects cultivated in those materials can be very useful to several areas of biomedical science including investigations of cell mechanical properties,[10,11] mechanosensitive ion channel signaling pathways,[12,13] targeted activation of specific ion channels,[14,15] and mechanical conditioning of cells for regenerative medicine applications.[16–18] Approaches utilizing magnetic-responsive materials and remote magnetic control can be grouped into three major categories. The first category includes applications in which magnetic particles attached to the cell membrane are manipulated using an externally applied time-varying gradient magnetic field. This approach has been used to generate forces in the piconewton range,[16] and has been applied to nanomagnetic actuation of receptor-mediated signal transduction[19] and mechanical cell conditioning for regenerative applications.[16–18] The second category covers polymeric magnetically responsive composite scaffolds developed to apply constant mechanical forces by an externally applied gradient field to modify the scaffold architecture and influence tissue regeneration, mainly in bone restoration applications.[20,21] The third category of applications is one that involves magnetically mediated drug release using magnetic scaffolds and externally applied gradient magnetic fields.[22,23] The common denominator for all these approaches is that the magnetic actuation or matrix deformations were obtained by using a non-uniform magnetic field resulting in field gradients. The role of field gradient is to impose volumetric force on the scaffold or a magnetic particle attached to the cell membrane, however using it *in vivo* can be problematic because gradient field magnitude depends on dimensions of the field creating device and distance to it.[24] For this reason, it would be desirable to perform magnetic actuation of the scaffolds without the requirement for magnetic field gradients.

Low frequency (below about 1 MHz) uniform magnetic fields are known for their ability to penetrate living tissues without limitations. Time-varying uniform magnetic fields coupled with magnetizable nanoparticles embedded within the scaffold can create transient physical forces transferrable to cells present in close proximity to the nanoparticles. Utilization of this feature for application of mechanical cues on cells in a remote way could enable cell stimulation in a non-invasive (noncontact) form, and therefore is highly useful for applications *in vivo*. The effect of mechanical stimuli was demonstrated in a wound healing model where mechanical cues from tissue tension generated during wound contraction promoted expansion of the vasculature as an integral part of the growing granulation tissue.[25] Our group has recently demonstrated the feasibility of remote stimulation induced by time-varying uniform magnetic fields in 3D cultures of endothelial and cardiac cells cultivated in alginate scaffolds impregnated with superparamagnetic nanoparticles.[26,27] We showed that remote stimulation of endothelial cells using a time-varying uniform magnetic field coupled with magnetic alginate scaffolds promotes the *in vitro* vessel-like organization of endothelial cells, an indicator of early vasculogenesis, which can potentially lead to generation of a pre-vascularized cellular graft.[26] Our previous results also point out to a synergistic effect of magneto-mechanical stimulation together with nanoparticulate features of the scaffold surface as providing a regenerative environment for cardiac cells driving their organization into functionally mature tissue.[27] The observed synergy of having both the magnetic nanoparticles and the time-varying uniform magnetic field indicates that direct effect of a uniform magnetic field was not the significant cause of the observed beneficial cell behavior. The conclusions leave the possibilities of mechanical deformations of the scaffold due to the applied magnetic field and, possibly, localized field gradients due to the magnetized nanoparticles in the scaffold as being the causes of the observations. Although these studies have demonstrated effects of the magnetic composite materials coupled with time-varying uniform magnetic fields on cells, the exact mechanism of stimulation is yet to be understood.

The primary goal of this paper is to investigate magneto-mechanical properties of a tissue engineered scaffold that could be employed for the purpose of remote mechanical stimulation *via* nearly uniform magnetic field. The work presented here can be viewed as a continuation of our previous work where time-varying uniform magnetic field was shown to have significant beneficial effects on cells developing in the same type of tissue engineered scaffold, but the possibility of mechanical deformations of the scaffold due to the uniform magnetic field was not studied. In this work the focus is on the understanding of mechanical deformation of the scaffold. Future work may address studies of localized magnetic field gradients in the scaffold.

In this study, we hypothesized, that a magnetically responsive scaffold can undergo a shape deformation due to alignment of scaffold's walls (containing superparamagnetic nanoparticles) even in a uniform magnetic field, creating bending/stretching forces that may exert a mechanical effect on the cells. To corroborate this hypothesis we have constructed a custom magnetic set-up adapted to an Atomic Force Microscope (AFM) that enabled application of time-varying uniform magnetic fields and monitored changes in matrix dimensions *in situ* as a function of applied magnetic field, concentration of magnetic particles within the scaffold wall structure and rigidity of the matrix. The collective observations from this study suggest a mechanistic explanation of potential mechanical effects generated in our magnetic materials. This work is our next step in understanding of how to accurately create proper stimulatory microenvironment for promotion of cellular organization to form mature tissue engineered constructs.

Experimental

Materials

Sodium alginate (LVG, 100 kDa, >65% guluronic acid) was obtained from NovaMatrix FMC Biopolymers (Drammen, Norway). Ferric chloride hexahydrate, ferrous chloride tetrahydrate, D-gluconic acid, hemicalcium salt and sodium hydroxide were obtained from Sigma-Aldrich (St. Louis, MO, USA). Phosphate buffered solution (PBS) and Dulbecco's modified eagle's medium (DMEM) supplemented with L-glutamine, 4.5 g per L glucose and sodium pyruvate was obtained from MediaTech (Manassas VA, USA), BenchMark™ heat inactivated fetal bovine serum (FBS) was obtained from Gemini Bio-Products (West Sacramento, CA, USA). Deionized water used in all experimental procedures was obtained using a Milli-Q water purification system. Alginate was modified with functional peptides RGD and heparin binding peptide (HBP) as was previously described.[28]

Magnetite preparation

Four batches of magnetite obtained from ferric chloride hexahydrate and ferrous chloride tetrahydrate (at a molar ratio 2 : 1, weighing 520 mg and 192 mg, respectively dissolved in 6.2 mL of doubly deionized water) by alkaline precipitation with aqueous sodium hydroxide (a 3.8 mL of 2 N sodium hydroxide) were magnetically separated and washed twice with 5 mL of water.[26,27] All four batches (maximal theoretical amount of 890 mg) of magnetite were combined and dispersed in 11 mL of 1.2% (w/v) alginate solution. The magnetite suspended in alginate solution was heated in a water bath (90 °C) for 20 min with a periodic mixing. Then the suspension was cooled down to a room temperature and sonicated for 5 min using an acoustic probe (0.5 inch diameter; 5 inch length) operated at 35–40% power corresponding to 190–220 Watts (550 Sonic Dismembrator, Fisher Scientific, USA) keeping the tube chilled on ice-water. The heating and sonication cycles were repeated twice resulting in a stable ferrofluid with a final magnetite concentration of ~8% (w/v). Particle size measurements were determined by Photon Correlation Spectroscopy (PCS) using a Delsa™ Nano C particle size analyzer equipped with two laser diodes (658 nm, 30 mW, Beckman-Coulter, CA, USA).

Fabrication of macroporous alginate scaffolds

Macroporous scaffolds, with a diameter of 5 mm and 7 mm thickness, were fabricated by a freeze-dry technique.[29] In brief, the alginates were dissolved in double distilled water (DDW) to obtain a 1.2% (w/v) solution, and then cross-linked by adding D-gluconic acid, hemicalcium salt (1.08% (w/v)), while stirring the mixture for achieving a uniform cross-linking of alginate. Magnetically responsive alginate scaffolds were fabricated using the same method from a mixture of alginate stabilized ferrofluid and alginate to obtain a relevant final concentration of magnetite post-crosslinking (*i.e.* 2.4%, 1.2%, 0.6% or 0.1% (w/v)). The cross-linked alginate solution was poured into 96-well plates (100 μL per well), chilled to 2–4 °C overnight, frozen at −20 °C for 24 h, and lyophilized. Scaffold sterilization was achieved by exposure to UV light for 1 hour in biological safety cabinet.

Characterization of scaffold morphology

Scaffold morphology was assessed by scanning electron microscopy (SEM; Zeiss model Supra 50VP). The dry scaffolds were attached to sample stubs with conductive paint and sputter-coated with an ultrathin (100 Å) layer of carbon using a Polaron E 5100 coating apparatus. The samples were visualized by SEM at an accelerating voltage of 12 kV.

Characterization of scaffold mechanical properties

Compressive modulus of wetted alginate scaffolds was tested with an Instron 4505 mechanical tester equipped with 100 N load cell. The scaffolds were wetted with culture medium for 2 days in a humidified atmosphere of 5% CO_2 and 95% air, at 37 °C. The crosshead speed was set at 2 mm min^{-1} for the Instron tester, and load was applied until the specimens were compressed to approximately 30% of the original thickness. Compressive modulus was calculated as the slope of the initial linear portion of the stress–strain curve. Three independent samples were analyzed in this series of tests.

Atomic force microscopy (AFM) measurement setup

The tested cylindrical scaffold was placed vertically (along its axial axis) in a non-compressible cylinder with an open upper side. A thin piece of mica was placed onto an upper side of the scaffold (held by capillary forces) to create a smooth surface, thus providing a flat landing pad (on an otherwise rough surface of the porous scaffold) for positioning of the AFM cantilever tip. The mica sheet collected forces generated from the movement of the scaffold pores, distributing the pressure to an AFM tip over a large area, representing a global change in scaffold height. The scaffold set up was placed in the center of a small custom made Helmholtz coils designed to fit measurements by the Dimension 3100 SPM with Nanoscope 4 controller equipped with DAFMLN open-loop scanner (Veeco) (Fig. 1). The Helmholtz coils were comprised from Perspex and made at the workshop of the Ben-Gurion University, Israel. The distance between the centers of the coils was 16 mm. Each coil was 4 mm thick, with an inner and outer diameter of 34 and 44 mm, respectively, and made of 200 turns of a 0.315 mm copper wire (Lion Electronics, Israel). In order to determine the field and field gradient in the coil, we used COMSOL Multiphysics software (Fig. 1) (COMSOL Inc., Palo Alto, CA, USA). The magnetic and electrical properties of the materials (air and copper) were obtained from the software material library. The measurements were conducted by an AFM using SCM-PIC probes (Pt–Ir coated Si-probe, k = 0.2 N m^{-1}, 450 μm long diving board cantilever, tip radius 20–25 nm) used for deflection measurements, RTESP (Si-probe, k = 40 N m^{-1}) for imaging the topography of the thin film surface in tapping mode. In our experiments two probe holders were used, the standard holder DAFMCH which has magnetic metallic components and the probe holder for SCM mode, DSCMSCH.

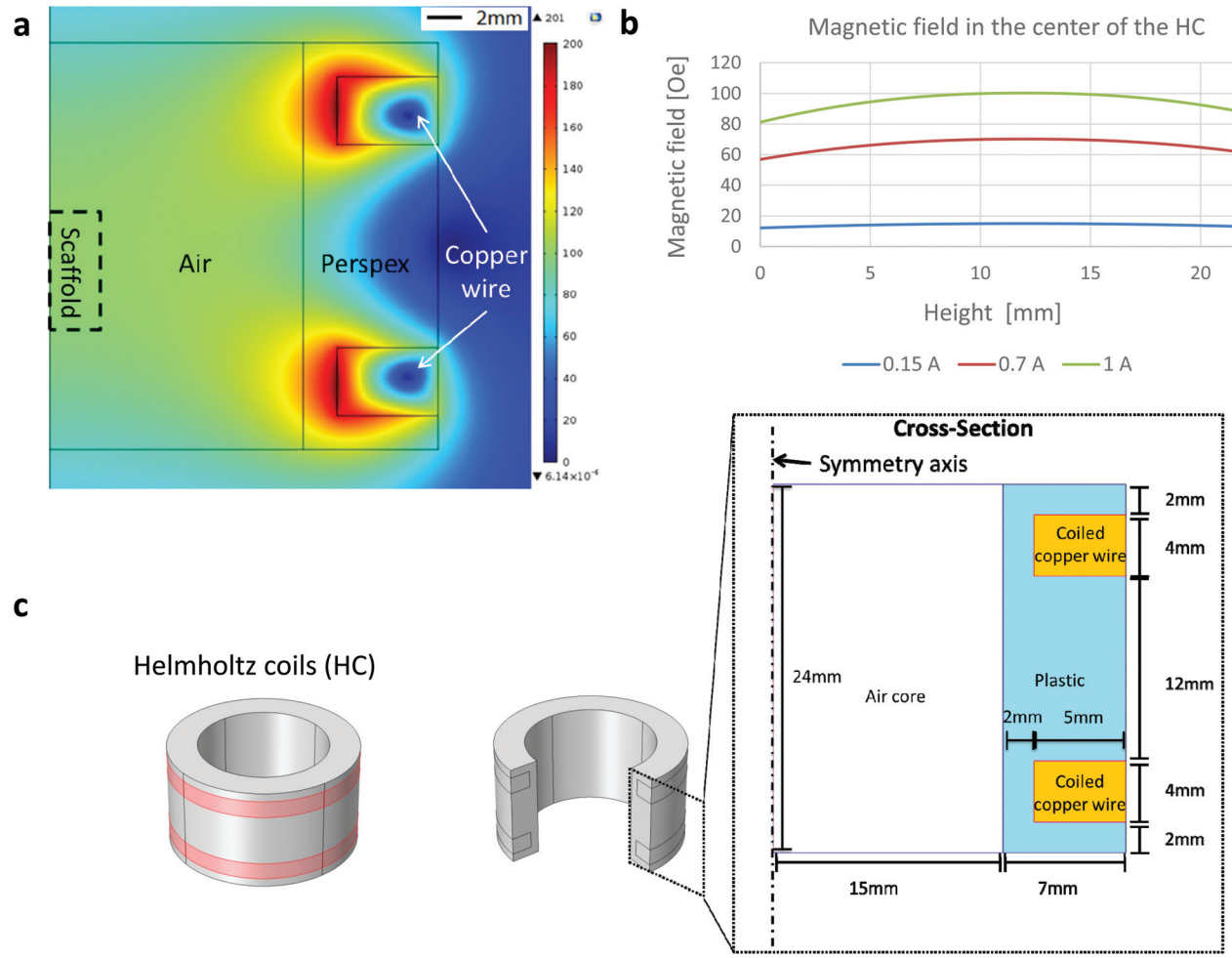

Fig. 1 The Helmholtz coils (HC) geometry and magnetic properties. (a) The magnetic field distribution in a cross section of the HC is described by a color bar for a current of 1 A passing through the coils. (b) The magnetic field distribution along the axis of the HC is described for currents of 0.15, 0.7, and 1 A passing through the coils. (c) The schematic representation of the HC structure and geometrical dimensions.

Statistics

Statistical analysis was performed with GraphPad Prism version 5.03 for Windows (GraphPad Software, San Diego, CA, USA). All variables are expressed as mean ± SEM from at least 3 independent experiments. To test the hypothesis when there were changes in various parameters over time among the experimental groups, a general linear 2-way ANOVA model was used. The model included the effects of treatment, time, and treatment-by time interaction. The Bonferroni's correction was used to assess the significance of predefined comparisons at specific time points. $P < 0.05$ was considered statistically significant.

Results

AFM setup design

To measure changes in matrix dimensions *in situ* we have designed and fabricated an original atomic force microscopy (AFM)-based setup, enabling to apply fairly uniform magnetic fields around the tested scaffold sample. The change of matrix dimensions is translated into changes of scaffold height in response to applied magnetic fields because the scaffold was positioned in a non-compressible cylinder with one open side. We assumed that due to its elasticity, scaffold's movement would be based on the ability of the scaffold (impregnated with MNPs) to align its structural elements (walls) along the lines of magnetic field upon magnetization. This situation is similar to a magneto-rheological fluid behavior where magnetic particles become polarized and align along the lines of a magnetic field.[30] In the case of MNP-impregnated alginate scaffold, the particles are locked within the polymeric matrix forming large magnetically responsive structures *i.e.* scaffold walls. Due to their anisotropic nature, the scaffold walls tend to align along the lines of magnetic field, thus changing the scaffold's dimensions. Assuming this potential mechanism, we hypothesized that a time-varying uniform magnetic field coupled with particles locked within scaffold's walls will lead

to a global deformation of the entire scaffold structure applying direct bending/stretching forces that exert a mechanical effect on the seeded cells within the matrix *i.e.* magneto-mechanical stimulation.

Our set-up is comprised of custom designed and made Helmholtz coils, with dimensions enabling the AFM cantilever tip to perform measurements on the moving surface of the scaffolds or hydrogels. In this set-up, the samples are placed inside a non-compressible cylinder (syringe piston), chosen to enable positioning the entire sample between the coils, while the height of the upper surface of the sample could be adjusted by moving the non-compressible cylinder plunger up or down. Positioning of the scaffold's set up along the axial dimension of the Helmholtz coils was done manually. The Helmholtz coils dimensions were designed to allow minimal variability in positioning the AFM scanner head inside the coils holder. Fairly uniform magnetic field generated by the coils at scaffold's position (Fig. 1) minimized potential variability due to manual calibration of the scaffold's set up positioning relatively to the coils. The cell culture medium could be easily added to wet the scaffolds and mimic our experimental conditions. A thin piece of mica was placed onto an upper side of the scaffold (held by capillary forces) to create a smooth surface, thus providing a flat landing pad (on an otherwise rough surface of the porous scaffold) for the AFM measurements. The mica collects forces from the global movement of the scaffold's pores, and distributes the pressure to the AFM tip over a large area, avoiding local damage or penetration of the AFM tip into the soft scaffold (Fig. 2).

Three dimensional deformation of material structure measured by AFM

In this part of our study, we have tested the AFM setup described above for its ability to monitor scaffold's response as a function of various conditions. The measurements were conducted under application of 1 Hz, square wave, time-varying uniform magnetic fields of 15 Oe, 70 Oe and 100 Oe. Each measurement included 20–30 cycles. In addition to testing the response of magnetic nanoparticle (MNP)-impregnated macroporous scaffolds to magnetic stimulation, we tested the behavior of MNP-impregnated hydrogels, to gain additional insights regarding the effects of matrix physical structure on particles and subsequent matrix response. The alginate hydrogel was obtained by calcium ion crosslinking in aqueous solution, while the macroporous solid scaffold is prepared by crosslinking followed by controlled freeze-drying.[29,31] The later process results in the formation of macro-porous alginate matrix, compared to the nano-size pores in the hydrogel.

The AFM measurements performed on hydrated MNP-impregnated macroporous alginate scaffolds showed that there was an increase in the height of these scaffolds, by up to 214 nm, which is about 0.003% change relative to the initial total scaffold's (1.2% MNP, 0.24% calcium) axial dimension in response to the 100 Oe magnetic field. In contrast, the height of the hydrogels consistently decreased, by up to 680 nm, corresponding to ~0.009% change relative to the initial total hydrogel axial dimension at the same experimental conditions (1.2% MNP, 0.24% calcium, 100 Oe, Fig. 3a and c respectively).

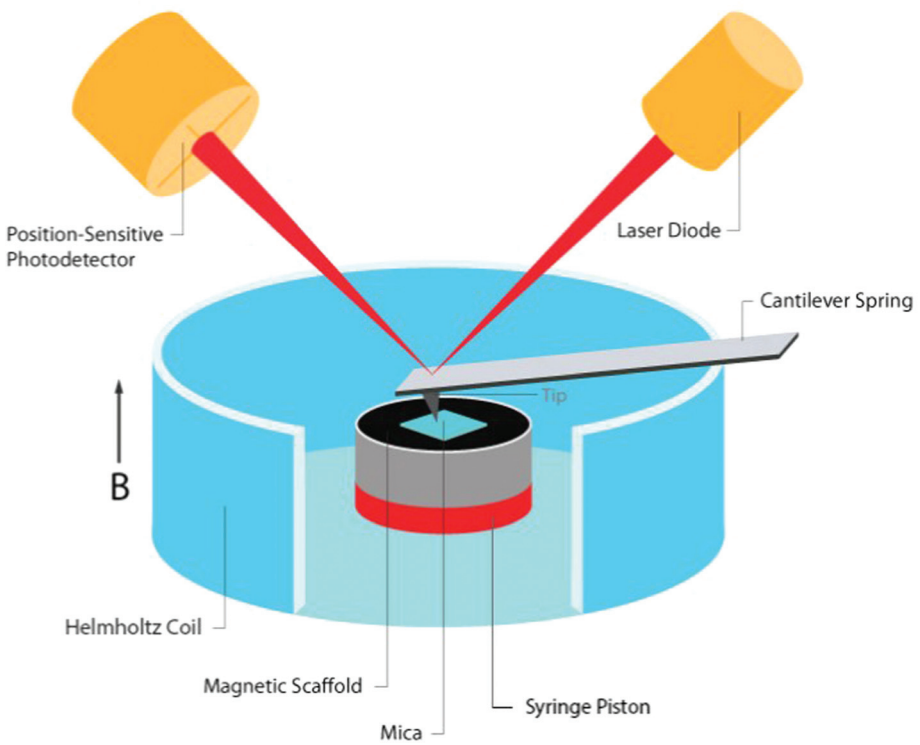

Fig. 2 A schematic overview of the AFM-based matrix height evaluation set-up.

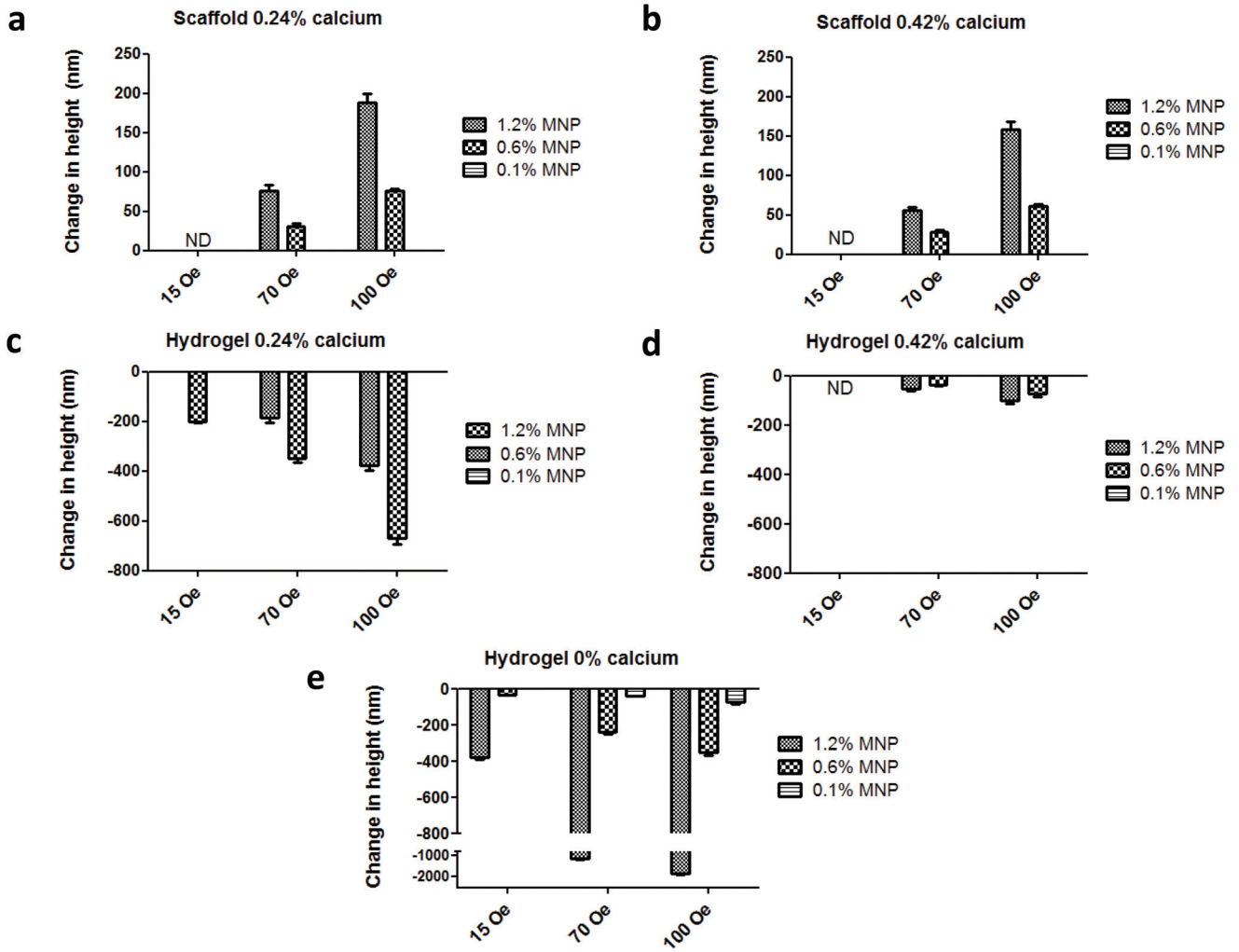

Fig. 3 Deformation of the matrix samples measured by AFM. Wetted macroporous (scaffold) and nanoporous (hydrogel) matrix height changes (scaffolds (a, b) and hydrogels (c–e)) were measured while magnetic field of 15 Oe, 70 Oe and 100 Oe was applied with frequency of 1 Hz. Each measurement included 20–30 cycles.

Moreover, our results clearly show that the percent change in matrix axial dimension is dependent on the concentration of MNPs embedded in both scaffolds and hydrogels. As expected, the magnitude of change in the scaffold/hydrogel height, in response to the magnetic field, depended on matrix rigidity/stiffness, as seen when comparing the scaffolds crosslinked with 0.42% and 0.24% (w/v) calcium ions. The more rigid scaffold crosslinked with 0.42% Ca^{2+} changed its height by a maximum of 160 ± 33 nm (~0.0023% change), while the change in the less rigid scaffold crosslinked with 0.24% Ca^{2+} was 214 ± 24 nm (~0.003% change), for the same maximal concentration of MNPs and applied field (1.2% (w/v), 100 Oe).

Similar behaviour was observed in hydrogels: 680 ± 27 (~0.009% change) and 120 ± 36 nm (~0.0017% change) for 0.24% (w/v) and 0.42% (v/w) calcium ion concentrations, respectively (MNP concentration 1.2% (w/v), field strength 100 Oe). Unfortunately, due to sensitivity limits of the AFM we were not able to measure scaffold height changes at 15 Oe, which is our experimental field condition in a typical cell stimulation experiment.[26,27] At this low magnetic field, sample movement could be visually observed, however because of the low signal-to-noise ratio the change in height could not be accurately measured. The AFM measurements also showed that the strongest response to a magnetic field in terms of scaffold height change was observed for the MNP-impregnated scaffolds prepared using calcium cross linker concentration of 0.24%, (w/v) and 1.2%, (w/v) MNPs. Comparing trends in the height change over 20 cycles of field application, we observed an interesting phenomena. The slope of the cycling curve for the hydrogel was about 5 times greater than that of the scaffolds, which indicates a distinct 3D structure and stiffness of the macroporous system of the scaffold when compared to the nanoporous hydrogel (Fig. 4a). The hydrogel group with no addition of the crosslinker presented pure ferrofluid behaviour within the magnetic field (Fig. 3e). We did not evaluate scaffolds with no addition of the crosslinker agent since this

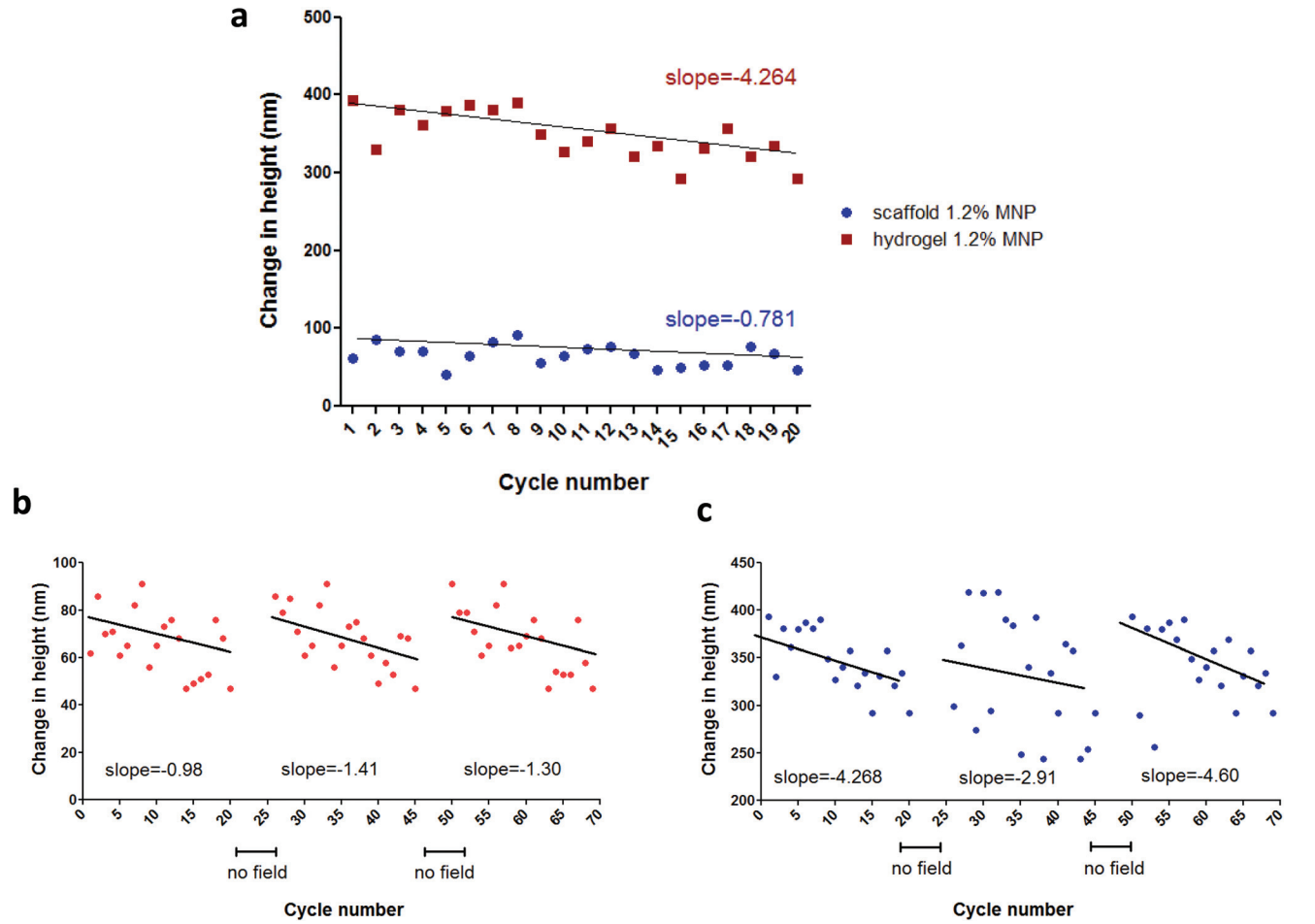

Fig. 4 (a) Deformation of the matrix samples measured by AFM over time during one stimulation interval (a representative measurement over 20 cycles). Deformation of the scaffold (b) and hydrogel (c) samples measured by AFM over three stimulation intervals (measurements in each stimulation interval were made over 20 cycles).

type of matrix post-wetting loses the macroporous nature, due to lack of strong bonds between the polymer chains. Non-impregnated with MNPs alginate scaffolds and hydrogels did not respond at all to a magnetic field as expected.

The deformation patterns over time (height change over multiple cycles of magnetic field application) show that both scaffolds and hydrogels demonstrated decreased response in height change with each cycle of stimulation as evidenced by a negative slope (Fig. 4). Yet, after a short period of relaxation time with no field application (>1 min), the height change magnitude of both scaffold and hydrogel samples recovered to its initial value (Fig. 4b and c). This result suggests that the frequency of an applied magnetic field used during the AFM test (approximately 1 Hz) was too high to allow a complete recovery of the material wall displacement, resulting in overall height magnitude decrease over the interval of 20 cycles of stimulation.

Scaffold morphology

In addition to characterization of material deformation we have thoroughly examined several scaffold parameters that could influence overall matrix response to an applied magnetic field. Scaffold morphology was studied by scanning electron microscopy (SEM) as a function of MNP concentration impregnated into the scaffold and concentration of calcium ion used for alginate crosslinking and scaffold formation. The highest studied final calcium concentration of 0.42% (w/v) for alginate crosslinking resulted in formation of alginate scaffold with relatively big "closed" pores interconnected with pores of a small size (mean pore size = 99 ± 19 μm). Lower calcium ion concentrations led to much more open pore structure with larger pores. Scaffolds prepared from 0.16% (w/v) calcium ions had a mean pore size of 133 ± 22 μm, appeared to be mechanically unstable and were tearing apart upon transfer. The scaffolds prepared with 0.24% (w/v) of calcium ion concentration, were mechanically stable in culture and had a mean pore size of 124 ± 33 μm.

Modulation of the MNP concentrations impregnated within the alginate scaffold walls also had an effect on scaffold appearance and morphology in terms of porosity and pore size (Fig. 5). The MNP content also significantly influenced the scaffold's wall topography. Scaffold impregnation with MNPs led to a formation of significantly larger

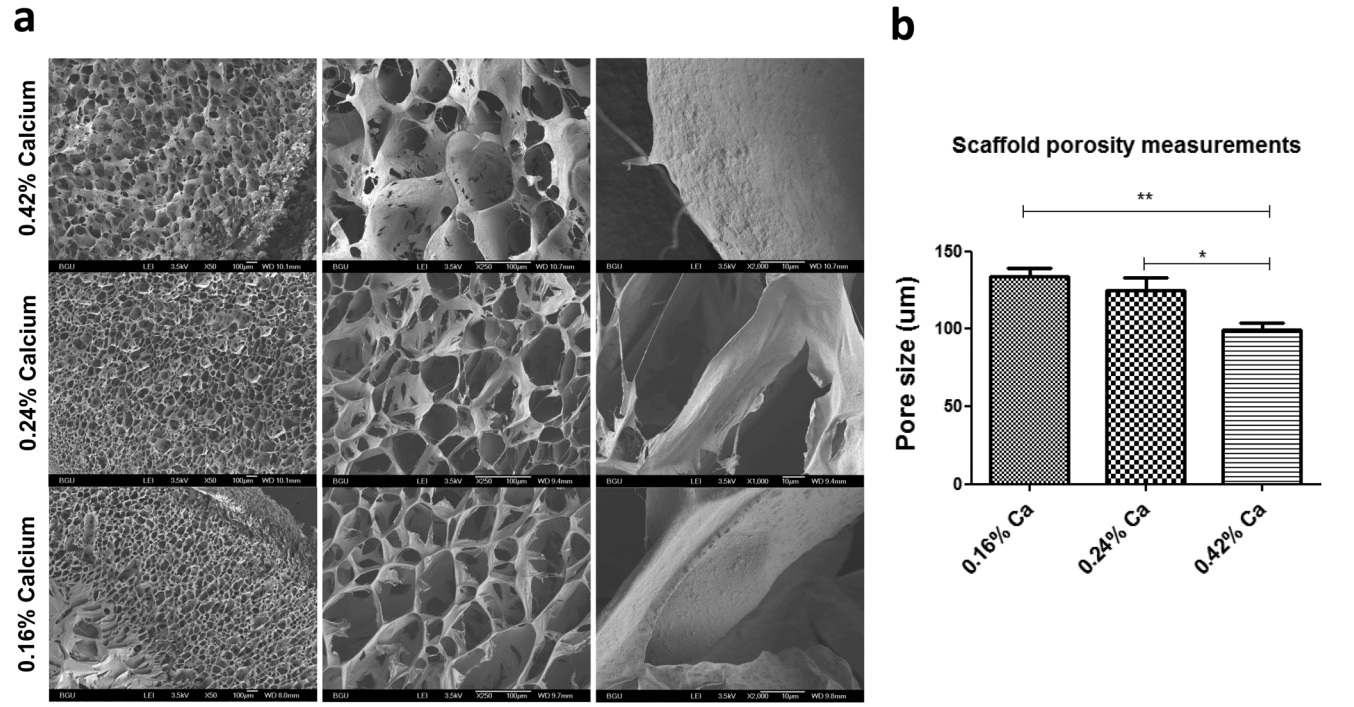

Fig. 5 Scaffold morphology: (a) scanning electron microscopy (SEM) of the magnetic scaffolds with different concentrations of the crosslinker (D-gluconic acid/hemi-calcium salt). (b) Scaffold porosity as function of crosslinker concentrations at 1.2% (w/v) MNP concentration.

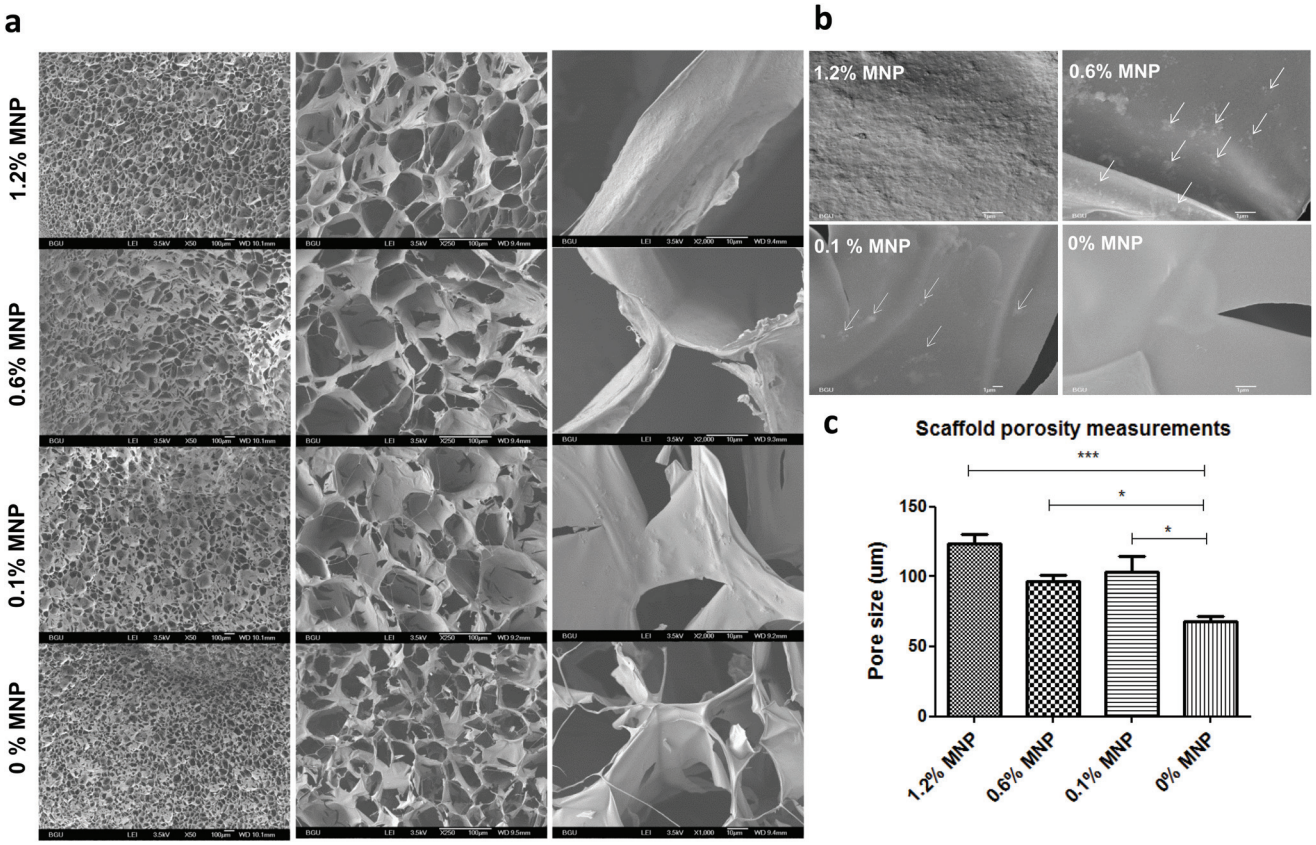

Fig. 6 Scaffold morphology: (a) scanning electron microscopy (SEM) of the scaffolds with different magnetic nanoparticle concentrations (fixed calcium concentration of 0.24% (w/v)). (b) Scaffold porosity measurements for variable magnetic nanoparticle concentrations.

pores compared with alginate scaffolds not loaded with MNPs. Interestingly, no statistical difference was found between different MNP-impregnated samples in terms of the pore size.

We also investigated scaffold wall topography to substantiate particle distribution and presentation on the wall surface, as this factor may play an important role in cell adhesion and interaction with the scaffold wall surface (Fig. 6). Because MNPs are surface-stabilized by alginate macromolecules they mix very well in alginate solution used for scaffold fabrication, leading to eventually homogeneous distribution and embedding of MNPs within the alginate matrix walls. The non-magnetic alginate scaffold displayed smooth matrix wall surface in contrast to a rough coarse-grain like one observed in MNP-impregnated scaffolds (Fig. 6b). At 1.2% (w/v) MNP loading the particles homogeneously distributed at the wall surface resulting in uniform material. At lower MNP concentrations (0.6 and 0.1% (w/v)), we observed few MNP aggregates in the scaffold walls positioned one from another at a distance much larger the aggregate size. Clumps or aggregates of MNPs not associated with scaffold's walls were not observed at all MNP concentrations. This observation indicates that alginate-coated MNPs interact well with the alginate matrix forming a homogeneous composite material.

Mechanical properties of the wetted scaffolds

We also examined whether incorporation of MNPs had influenced mechanical properties of wetted macroporous scaffolds. To this end, we've examined wetted alginate scaffolds containing various MNP concentrations by measuring Young's modulus (a measure of the stiffness of an elastic material) using Instron system operated in a compression mode. Fig. 7 shows that incorporation of MNPs within the walls of alginate

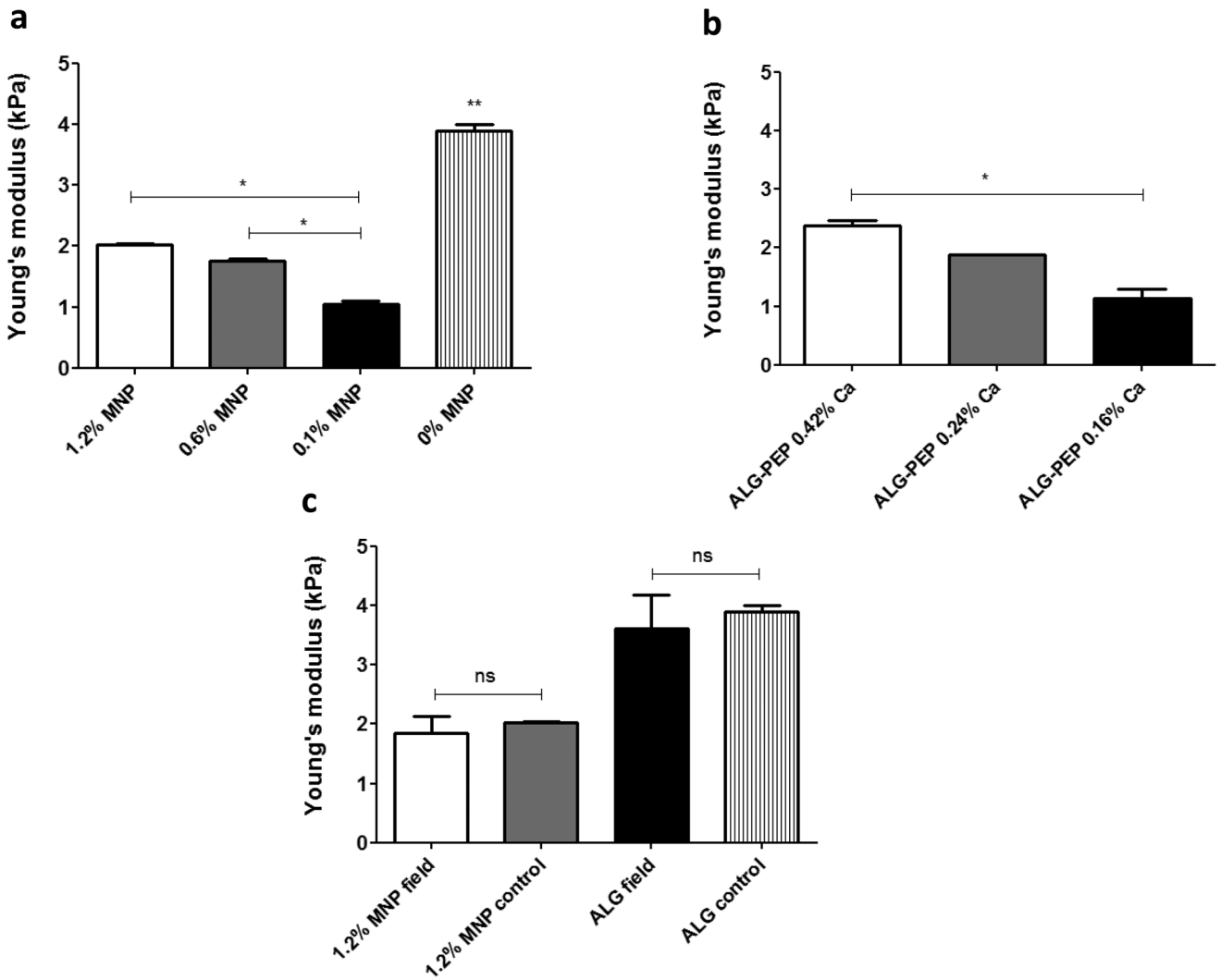

Fig. 7 Mechanical properties of scaffolds (prepared by cross-linking and then freeze-drying process). (a) Young's modulus of scaffolds at various MNP concentrations, (b) Young's modulus of scaffolds at various concentrations of the crosslinker, (c) Young's modulus of scaffolds cultivated for 7 days with and without exposure to a magnetic stimulation. Asterisks denote significant differences (by one way ANOVA) *$p < 0.05$, **$p < 0.01$ and ***$p < 0.005$).

scaffolds dramatically lowered matrix stiffness as compared to the alginate scaffold not loaded with MNPs. It is of note that in MNP-impregnated scaffolds, an increase in MNP concentration resulted in increase of the alginate matrix stiffness, possibly due to a stiff nature of the magnetite nanocrystals (Fig. 7a). As expected, increasing the concentration of the calcium ion cross-linker has resulted in stiffer scaffold (Fig. 7b).

We further tested whether magnetic stimulation over time affects the stiffness of scaffolds incubated in cell culture medium. After a stimulation period of one week, which is an analogous to a stimulation time frame in our cell stimulation experiments,[26] no significant difference in matrix stiffness have been found between the magnetically stimulated and the non-stimulated (control) scaffold groups in both MNP-impregnated and non-impregnated alginate scaffolds (Fig. 7c). This points out that the stimulation process *per se* has no significant effect on scaffold's macroporous structure and its mechanical properties.

Discussion

Preparation of pre-vascularized functional tissues requires formation of proper chemical and physical environments. Magnetically responsive biomaterials are highly attractive for generation of remotely activated physical cues on cells because a magnetic field can penetrate living tissues without limits. Uniform magnetic fields coupled with magnetically responsive elements (*e.g.* magnetic nanoparticles) embedded within the elastic biomaterial structure can controllably generate magnetic forces responsible for application of a direct mechanical stimulus on cells cultivated within the biomaterial. This capability is particularly important when mechanical stimulation is desired *in vivo* while other methods cannot be used since they require a direct contact with the stimulated tissue.[32,33]

Our group develops magnetically responsive alginate scaffolds for remote application of physical cues to the cultivated cells as a complementary strategy for biochemical stimulation. The uniqueness and novelty of our tissue engineered scaffolds and remote cell stimulation approach is in the ability to generate mechanical cues using time-varying uniform magnetic fields. The remote application of physical cues *in vivo* is of high potential to achieve more rapid and efficient integration of the implanted cell construct with the host tissue. Generation of uniform magnetic fields across large animals or even humans is a relatively easy and scalable task, as opposed to situations where gradient fields are used for the same purpose. This distinction makes our approach highly important for the future clinical translation. We have recently demonstrated the feasibility of physical stimulation induced by uniform magnetic fields in 3D cultures of endothelial and cardiac cells cultivated in magnetic alginate scaffolds.[26,27] However, the mechanism of cell stimulation in these studies was not determined. In addition to possible mechanical *i.e.* 'magneto-mechanical' effect (formation of mechanical force due to scaffold deformation in response to a magnetic field), magnetic field, mechanical vibration, scaffold surface topography and scaffold chemical composition can be other effectors of cellular behavior in our scaffolds. Although it is very likely that the observed cellular responses to stimulation in our alginate scaffolds result from a combination of all the above factors, the contribution of mechanical stimulation could be the most significant through activation of mechanosensitive pathways.[34–36] Thus, the goal of the present study was to experimentally assess feasibility of 'magneto-mechanical' stimulation and attempt estimate the order of magnitude of this effect. We hypothesized that magnetic scaffold exposed to a time-varying uniform magnetic field can undergo a reversible (elastic) 3D structure deformation due to magnetization of superparamagnetic nanoparticles (MNPs) immobilized within the structure and scaffold wall alignment. The alternating pattern of scaffold wall alignment and relaxation is expected to create bending/stretching forces that can exert a mechanical effect on the cells. The ability of magnetic alginate scaffold to change its dimensions in response to a remotely applied time-varying uniform magnetic field was confirmed using a specially designed set-up adapted to an Atomic Force Microscope, AFM (Fig. 2). This setup enabled us to utilize the capability of AFM to monitor changes of sample dimensions *via* measuring changes in surface height as a result of collective response of MNPs leading to a 3D deformation of the scaffold. The behavior of magnetic particles exposed to a magnetic field in liquid media is well characterized.[30] In magnetic field, particles acquire magnetic moment and align along the lines of a magnetic field forming chains. Our results show that both macro- and nanoporous matrix structures (scaffolds and hydrogels respectively) inversely change their dimensions in response to a magnetic field, demonstrating elongation of the scaffold structure (positive height change) *versus* shrinkage in hydrogels (negative height change). Although both scaffolds and hydrogels are defined as semi-solid materials, their opposing response indicates on a different degree of MNP association with matrix walls. Alginate scaffolds and hydrogels were prepared similarly, except for the freeze-drying process: a differentiating step that leads to formation of macroporous structure and apparently stronger MNP immobilization within the matrix material. During the freeze-drying process, the alginate polymer chains strongly connect by numerous van der Waals bonds and possibly "lock" MNPs within the resulting scaffold walls, while microscopic ice crystals (later to become pores) are formed.[29] Wetting this type of matrix makes it to appear and behave like a hydrogel; however the strong bonds between polymer chains remain stable and do not brake after hydration. Because of stiff nature of the scaffolds it is reasonable to assume that magnetically induced particle movement in this type of matrix will be limited and mainly associated with the movement of the scaffold wall. The elongation of scaffolds (positive height increase) per AFM measurements is consistent with this assumption indicating that locked within scaffold walls MNPs cause scaffold walls to align. Hydrogel, lacking the stiff nature, enables particles to more significantly distort polymeric structure and move more freely perhaps

creating chains or aggregates upon magnetization. Because MNPs are stabilized by alginate macromolecules, the entire hydrogel structure shrinks when particle movement is initiated, consequently causing a decrease in the hydrogel height. Fig. 8 schematically proposes an explanation for the mechanism of matrix elongation in the scaffold and shrinkage in the hydrogel.

The phenomenon of scaffold deformation was observed in a dose-dependent manner as a function of applied magnetic field, particle concentration, and matrix mechanical properties. Higher concentrations of MNPs as well as stronger magnetic field (one-to-two orders of magnitude lower than MNP saturation magnetization field) led to stronger interactions between magnetized particles and as a result to a more significant deformation of the matrix. Interestingly, scaffold's stiffness was also altered by the presence of MNPs in the matrix walls and seemed to additionally influence the response of the entire system. The MNP-impregnated scaffolds appear to be significantly more elastic and less stiff, when compared to the non-loaded ones. Elastic response and stiffness of the scaffolds are greatly influenced by the existing interactions between polymer molecules, molecule branching and complexity of these interactions. Crosslinking of alginate by divalent calcium ions and the resulting "egg-box model" is dose-dependent. By adding higher amounts of crosslinking agent (calcium ions) polymer chains are linked tighter, which strengthens the van der Waals forces between the chains, thus restricting their movement and reducing elasticity. The steric hindrance due to incorporation of MNPs between the polysaccharide chains is possibly the reason for the increased elasticity and decreased stiffness of the magnetic scaffolds. Magnetite crystal aggregates are significantly bigger than individual alginate molecules, therefore it is likely that they will interfere the in the "egg-box" crosslinking between the polymer chains resulting in more elastic matrix compared to the control, non-loaded with MNPs scaffold.

Although the magnetic nanoparticles have multiple strong surface interactions with cross-linked alginate molecules tightly associated with scaffold's walls, the uptake of nanoparticles by cells is possible, which may raise some safety concerns. In our recent studies, we demonstrated that active loading of primary endothelial cells with MNPs at doses necessary for magnetic cell targeting (about 25 pg magnetite per cell) did not adversely affect cellular function, gene expression, metabolic and structural cell integrity.[37,38] Despite that, the expected potential uptake of nanoparticles in magnetic scaffolds could be significantly lower than in actively MNP-loaded cells, this situation warrants future investigation to validate that MNP-uptake is negligible and has insignificant effects on cells.

It is of note that the analysis of height changes over time has revealed an interesting trend. The changes in matrix elongation became smaller with increase in cycle number of field application resulting in a negative trend for both scaffolds and hydrogels (Fig. 5). This behavior suggests either change in matrix response or change in material structure. Repetition of these experiments with cessation in field application enabling the samples to recover between measurement sets (>1 min) revealed that after a period of recovery the magnitude returned to its initial values. This result suggests that material is elastic, its structure doesn't change and that the frequency of stimulation used for these measurements (~1 Hz) is too high for the sample to fully recover during repeatable field application. This implies that in biological scenario, the continuous stimulation will result in slightly reduced amplitude of scaffold response.

Although the nanoparticles embedded in the scaffold walls are not conductive and do not have remnant magnetization, they can absorb some of the energy associated with the magnetization and convert it to heat. This is due to the fact that a phase lag between the nanoparticle magnetization and the external magnetic field is possible. For nanoparticles that are not free to move, such phase lag occurs primarily through so-called Neel relaxation of the nanoparticles' magnetic moments. This effect has been suggested, in fact, as a possible mechanism for hyperthermia treatment.[39] For individual nanoparticles of diameters around 20–30 nm, Neel relaxation occurs on the time scale longer than 1 ms. Therefore, for such isolated nanoparticles, very little heating is expected at frequencies below about 1 kHz. Although, in the scaffold, magnetostatic interactions between the nanoparticles can significantly increase the relaxation time making heating at

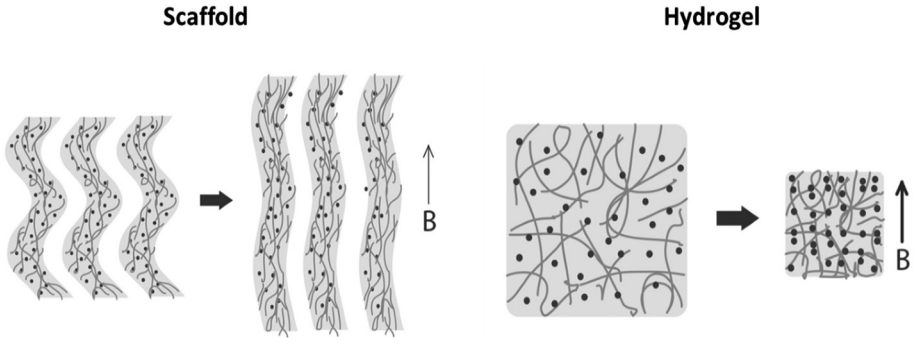

Fig. 8 A proposed mechanism of the matrix deformation within a magnetic field.

frequencies below 100 Hz theoretically possible, the heating was not observed in our experiments.

The mechanical force threshold required to tip the state of the cellular components is small. It has been shown that less than 0.2 pN was required to activate the TREK-1 channel[15] and 2 pN to break the bond between fibronectin and the cytoskeleton.[40] Activation of downstream calcium signaling has been fulfilled with forces of 8–10 pN using optical tweezers.[41] The force applied to MNPs attached to cell receptors using magnetic force bioreactor (MFB) for conditioning of cells was estimated to be in the range of 0.2–2 pN per particle,[17] which resulted in an increase in tyrosine phosphorylation after 30 min upon magnetic stimulation in $PDGFR_{\alpha}$ targeting group. To estimate the order of magnitude of mechanical forces developed in our scaffolds as a result of scaffold deformation, and potentially acting on cells we propose the following calculation. The force, F exerted by stretched or contracted material can be estimated using an equation derived from the Hooke's law: $F = \frac{EA_o\Delta L}{L_o}$, where E is the Young's modulus (modulus of elasticity), A_o is the original cross-sectional area through which the force is applied, ΔL is the amount by which the length of the object changes, and L_o is the original length of the object. In our case, the stretched object is a living cell with dimensions of 20 × 20 × 5 μm that is adhered to the scaffold wall. We consider a scenario when a cell is being stretched along one of its larger dimensions (20 μm). In this situation the cross sectional area through which the force is applied would be 10^{-10} m^2 (A_o). The majority of publications that employed AFM approach to measure cell mechanics determine a value for Young's (elastic) modulus in the range from few hundred of Pa to tens of kPa.[42] For example the elastic modulus of human umbilical vein endothelial cells (HUVECs) was determined to be in the range of 1.3–7.2 kPa,[43] 3–12 kPa for fibroblasts,[44] 11–45 kPa for skeletal muscle cells[45] and 90–110 kPa for cardiomyocytes.[46] Although we could not measure scaffold elongation at the typical field of 15 Oe used in our cell culture experiments,[26,27] we can estimate it as about 10 nm (ΔL). The initial scaffold length along its axial direction was 7 mm (L_o). Using Young's modulus of 7 kPa for endothelial cells and substituting all the above values into the force equation we obtain force potentially acting on a cell in a typical cell culture stimulation experiment in the order of 1 pN. It may be worth noting that, when this force is used to estimate energy associated with cell deformation based on the cell dimensions and a Young's modulus of 1–10 kPa, one finds this energy to be below kT, the energy of thermal fluctuations (k is the Boltzmann's constant and T is temperature in Kelvin). Based on this one might be tempted to discount the effect of mechanical stimulus associated with 1 pN forces on cells. However, the fact that forces of this magnitude acting on cells have been observed to have substantial effects on cell behavior as mentioned above[17,41] suggests that such forces may shift balance between various non-equilibrium cellular processes. Thermal fluctuation forces are highly randomized and local. The probability that these forces will act on every unit of the scaffold simultaneously is considerably low. Furthermore, in a tissue engineered scaffold as in other bioreactor-type experiments,[17] weak mechanical forces act on different cells in a highly correlated manner and can affect variety of processes at a cell culture level. These may be some of the reasons why mechanical forces weaker than thermal fluctuation forces acting on individual cells may have been observed to affect cell behavior significantly.

It is additionally noteworthy that the estimated forces were measured in the scaffolds lacking cells. The presence of cells forming focal adhesions may increase the Young's modulus of the entire cell construct. The estimated force of 1 pN in the cell-free scaffolds seems to be much higher than the reported threshold (as little as 0.2 pN[15]) required to induce cellular mechanotransduction. One might expect that in the cell-seeded scaffolds the developed forces may still be sufficient to induce a beneficial cellular response. Moreover, our current results indicate that the applied forces can be increased through application of stronger magnetic fields. This strategy can enable finding appropriate mechanical stimulatory force condition in a real cell construct environment in the future stimulatory condition optimization studies.

While this study indicates on possibility of generating bending/stretching forces that may exert a mechanical effect on cells, there is also a possibility of generating mechanical vibration of small magnitude when anisotropic magnetic scaffold is exposed to an alternating magnetic field in a typical cell stimulation setting. Considerable experimental evidence shows that mechanical vibration influence cellular structure and various processes such as viability, proliferation, adhesion, and differentiation. The effects of mechanical vibration on cell activity and behavior remain controversial. There has been evidence of both positive and negative effects on cell and organism levels. Recently, novel approaches were developed to destroy cancer cells producing low frequency mechanical vibration effects on the cancer cell membrane or cytosol. In these studies, anisotropic magnetic particles were used to exert forces or torques inducing cell apoptosis or necrosis.[47–53] Mechanical vibration has been shown to control cell adhesion[54,55] and proliferation.[56–59] Furthermore, mechanical vibration has been shown to direct osteogenic differentiation and promote bone formation,[58–65] while restricting mesenchymal stem cell adipogenic commitment.[66] Although the diverse effects of mechanical vibration on cells were observed at a variety of conditions, the implications of such effects should be carefully considered and studied in each specific experimental scenario.

It is likely that mechanical forces developed as a result of scaffold deformation would be less concentrated compared to the magnetic microspheres attached to cellular receptors, where the force is concentrated roughly over the cross-sectional area of the microsphere. For this reason, the realistic force acting on cells in magnetic scaffolds could be lower than estimated. However even making this assumption, the realistic forces could be still in the range being able to induce mechanotransduction effects on a cellular or cellular organelle level. Nonetheless, additional research is needed to investigate

whether developed forces can be applied to cells at a relevant level to promote efficient integration of the cell construct with host tissue upon implantation.

Conclusions

The present study provides experimental evidence for a reversible 3D deformation of magnetically responsive scaffolds exposed to an externally applied time-varying uniform magnetic field. The matrix structure deformation is produced by immobilized magnetic nanoparticles within the matrix walls resulting in collective alignment of scaffold walls upon magnetization. Our data indicates on possibility of generating bending/stretching forces that may exert a mechanical effect on cells due to alternating pattern of scaffold wall alignment and relaxation. The matrix deformation is reversible which suggest that the structure of the matrix doesn't change. The estimated mechanical force that can be imparted on cells in the order of 1 pN is in good agreement with reported threshold to induce mechanotransduction effects on cellular level. This mechanistic insight is valuable for interpretation of cellular responses within magnetic alginate scaffolds and can be further used for optimization of applied forces for cell stimulation.

Acknowledgements

Yulia Sapir gratefully acknowledges the Azrieli Foundation for awarding the Azrieli Fellowship supporting her PhD program. The study was partially supported by The Louis and Bessie Stein Family foundation through the Drexel University College of Medicine (BP, YS, SC), American Associates of the Ben-Gurion University of the Negev, Israel (YS), Drexel University College of Medicine Clinical & Translational Research Institute (CTRI) (BP), a grant from The W.W. Smith Charitable Trust (award number H1504) (BP), and the National Heart, Lung and Blood Institute (award number R01HL107771) (BP). The content is solely the responsibility of the authors and does not necessarily represent the official views of the National Heart, Lung and Blood Institute or the National Institutes of Health.

Professor Cohen holds the Claire and Harold Oshry Professor Chair in Biotechnology.

References

1 C. Basavaraja, J. K. Kim and D. S. Huh, *Polym. Compos.*, 2014, **35**, 2010–2017.
2 R. Glaser, V. Caccese and M. Shahinpoor, *Smart Mater. Struct.*, 2011, 20.
3 W. H. Guo, C. Liu, X. M. Sun, Z. B. Yang, H. G. Kia and H. S. Peng, *J. Mater. Chem.*, 2012, **22**, 903–908.
4 J. A. Verduzco, I. Betancourt, N. Ortiz, L. R. Olmos and J. Garcia, *Mater. Lett.*, 2006, **60**, 2033–2037.
5 R. F. Ziolo, E. P. Giannelis, B. A. Weinstein, P. O'Horo, M. B. N. Ganguly, V. Mehrotra, M. W. Russell and D. R. Huffman, *Science*, 1992, **257**, 219–223.
6 J. Dobson, *Nat. Nanotechnol.*, 2008, **3**, 139–143.
7 J. de Vicente, D. J. Klingenberg and R. Hidalgo-Alvarez, *Soft Matter*, 2011, **7**, 3701–3710.
8 G. Bossis, S. Lacis, A. Meunier and O. Volkova, *J. Magn. Magn. Mater.*, 2002, **252**, 224–228.
9 X. Tang, X. Zhang, R. Tao and Y. M. Rong, *J. Appl. Phys.*, 2000, **87**, 2634–2638.
10 D. E. Ingber, *FASEB J.*, 2006, **20**, 811–827.
11 N. Wang, K. Naruse, D. Stamenovic, J. J. Fredberg, S. M. Mijailovich, I. M. Toric-Norrelykke, T. Polte, R. Mannix and D. E. Ingber, *Proc. Natl. Acad. Sci. U. S. A.*, 2001, **98**, 7765–7770.
12 L. J. Santos, R. L. Reis and M. E. Gomes, *Trends Biotechnol.*, 2015, **33**, 471–479.
13 N. J. Sniadecki, *Endocrinology*, 2010, **151**, 451–457.
14 S. Hughes, A. J. El Haj and J. Dobson, *Med. Eng. Phys.*, 2005, **27**, 754–762.
15 S. Hughes, S. McBain, J. Dobson and A. J. El Haj, *J. R. Soc. Interface*, 2008, **5**, 855–863.
16 S. H. Cartmell, A. Keramane, G. R. Kirkham, S. B. Verschueren, J. L. Magnay, A. J. El Haj and J. Dobson, *J. Phys.: Conf. Ser.*, 2005, **17**, 77–80.
17 J. Dobson, S. H. Cartmell, A. Keramane and A. J. El Haj, *IEEE Trans. Nanobioscience*, 2006, **5**, 173–177.
18 J. M. Kanczler, H. S. Sura, J. Magnay, D. Green, R. O. C. Oreffo, J. P. Dobson and A. J. El Haj, *Tissue Eng., Part A*, 2010, **16**, 3241–3250.
19 R. J. Mannix, S. Kumar, F. Cassiola, M. Montoya-Zavala, E. Feinstein, M. Prentiss and D. E. Ingber, *Nat. Nanotechnol.*, 2008, **3**, 36–40.
20 A. Russo, S. Panseri, T. Shelyakova, A. Parrilli, M. Sandri, A. Ortolani, M. Bianchi, A. Tampieri, V. Dediu, M. Santin and M. Marcacci, *Tissue Eng., Part A*, 2015, **21**, S17–S17.
21 S. Panseri, A. Russo, M. Sartori, G. Giavaresi, M. Sandri, M. Fini, M. C. Maltarello, T. Shelyakova, A. Ortolani, A. Visani, V. Dediu, A. Tampieri and M. Marcacci, *Bone*, 2013, **56**, 432–439.
22 S. H. Hu, T. Y. Liu, D. M. Liu and S. Y. Chen, *J. Controlled Release*, 2007, **121**, 181–189.
23 X. Zhao, J. Kim, C. A. Cezar, N. Huebsch, K. Lee, K. Bouhadir and D. J. Mooney, *Proc. Natl. Acad. Sci. U. S. A.*, 2010, **108**, 67–72.
24 B. Polyak and G. Friedman, *Expert Opin. Drug Delivery*, 2009, **6**, 53–70.
25 W. W. Kilarski, B. Samolov, L. Petersson, A. Kvanta and P. Gerwins, *Nat. Med.*, 2009, **15**, 657–664.
26 Y. Sapir, S. Cohen, G. Friedman and B. Polyak, *Biomaterials*, 2012, **33**, 4100–4109.
27 Y. Sapir, B. Polyak and S. Cohen, *Nanotechnology*, 2014, **25**, 014009.
28 Y. Sapir, O. Kryukov and S. Cohen, *Biomaterials*, 2011, **32**, 1838–1847.
29 L. Shapiro and S. Cohen, *Biomaterials*, 1997, **18**, 583–590.

30 P. Poddar, J. L. Wilson, H. Srikanth, J. H. Yoo, N. M. Wereley, S. Kotha, L. Barghouty and R. Radhakrishnan, *J. Nanosci. Nanotechnol.*, 2004, **4**, 192–196.
31 S. Zmora, R. Glicklis and S. Cohen, *Biomaterials*, 2002, **23**, 4087–4094.
32 L. L. Chiu, R. K. Iyer, J. P. King and M. Radisic, *Tissue Eng., Part A*, 2011, **17**, 1465–1477.
33 T. Dvir, O. Levy, M. Shachar, Y. Granot and S. Cohen, *Tissue Eng.*, 2007, **13**, 2185–2193.
34 C. J. Meyer, F. J. Alenghat, P. Rim, J. H. Fong, B. Fabry and D. E. Ingber, *Nat. Cell Biol.*, 2000, **2**, 666–668.
35 N. Wang, J. P. Butler and D. E. Ingber, *Science*, 1993, **260**, 1124–1127.
36 N. Wang and D. E. Ingber, *Biochem. Cell Biol.*, 1995, **73**, 327–335.
37 Z. Orynbayeva, R. Sensenig and B. Polyak, *Nanomedicine*, 2015, **10**, 1555–1568.
38 F. T. Zohra, M. Medved, N. Lazareva and B. Polyak, *Nanomedicine*, 2015, **10**, 1391–1406.
39 J. P. Fortin, F. Gazeau and C. Wilhelm, *Eur. Biophys. J.*, 2008, **37**, 223–228.
40 G. Jiang, G. Giannone, D. R. Critchley, E. Fukumoto and M. P. Sheetz, *Nature*, 2003, **424**, 334–337.
41 L. M. Walker, A. Holm, L. Cooling, L. Maxwell, A. Oberg, T. Sundqvist and A. J. El Haj, *FEBS Lett.*, 1999, **459**, 39–42.
42 T. G. Kuznetsova, M. N. Starodubtseva, N. I. Yegorenkov, S. A. Chizhik and R. I. Zhdanov, *Micron*, 2007, **38**, 824–833.
43 A. B. Mathur, G. A. Truskey and W. M. Reichert, *Biophys. J.*, 2000, **78**, 1725–1735.
44 C. Rotsch, F. Braet, E. Wisse and M. Radmacher, *Cell Biol. Int.*, 1997, **21**, 685–696.
45 A. M. Collinsworth, S. Zhang, W. E. Kraus and G. A. Truskey, *Am. J. Physiol. Cell Physiol.*, 2002, **283**, C1219–C1227.
46 A. B. Mathur, A. M. Collinsworth, W. M. Reichert, W. E. Kraus and G. A. Truskey, *J. Biomech.*, 2001, **34**, 1545–1553.
47 M. N. Bouchlaka, G. D. Sckisel, D. Wilkins, E. Maverakis, A. M. Monjazeb, M. Fung, L. Welniak, D. Redelman, A. Fuchs, C. A. Evrensel and W. J. Murphy, *PLoS One*, 2012, **7**, e48049.
48 D. Cheng, X. Li, G. Zhang and H. Shi, *Nanoscale Res. Lett.*, 2014, **9**, 195.
49 D. H. Kim, E. A. Rozhkova, I. V. Ulasov, S. D. Bader, T. Rajh, M. S. Lesniak and V. Novosad, *Nat. Mater.*, 2010, **9**, 165–171.
50 D. Liu, L. Wang, Z. Wang and A. Cuschieri, *Nano Lett.*, 2012, **12**, 5117–5121.
51 E. A. Vitol, V. Novosad and E. A. Rozhkova, *IEEE Trans. Magn.*, 2012, **48**, 3269–3274.
52 E. Zhang, M. F. Kircher, M. Koch, L. Eliasson, S. N. Goldberg and E. Renstrom, *ACS Nano*, 2014, **8**, 3192–3201.
53 S. Leulmi, X. Chauchet, M. Morcrette, G. Ortiz, H. Joisten, P. Sabon, T. Livache, Y. Hou, M. Carriere, S. Lequien and B. Dieny, *Nanoscale*, 2015, **7**, 15904–15914.
54 W. S. Nishitani, A. M. Alencar and Y. Wang, *PLoS One*, 2015, **10**, e0126440.
55 S. Trierweiler, H. Holmes, B. Pereles, R. Rajachar and K. G. Ong, *J. Biomed. Sci. Eng.*, 2013, **6**, 478–482.
56 Y. Y. Jiang, J. K. Park, H. H. Yoon, H. Choi, C. W. Kim and Y. K. Seo, *Prep. Biochem. Biotechnol.*, 2015, **45**, 476–490.
57 J. A. Kaupp and S. D. Waldman, *Proc. Inst. Mech. Eng., Part H*, 2008, **222**, 695–703.
58 C. Zhang, J. Li, L. Zhang, Y. Zhou, W. Hou, H. Quan, X. Li, Y. Chen and H. Yu, *Arch. Oral Biol.*, 2012, **57**, 1395–1407.
59 C. Zhang, Y. Lu, L. Zhang, Y. Liu, Y. Zhou, Y. Chen and H. Yu, *Arch. Med. Sci.*, 2015, **11**, 638–646.
60 E. Lau, W. D. Lee, J. Li, A. Xiao, J. E. Davies, Q. Wu, L. Wang and L. You, *J. Orthop. Res.*, 2011, **29**, 1075–1080.
61 D. Pre, G. Ceccarelli, G. Gastaldi, A. Asti, E. Saino, L. Visai, F. Benazzo, M. G. Cusella De Angelis and G. Magenes, *Bone*, 2011, **49**, 295–303.
62 D. Pre, G. Ceccarelli, L. Visai, L. Benedetti, M. Imbriani, M. G. Cusella De Angelis and G. Magenes, *Bone Marrow Res.*, 2013, **2013**, 803450.
63 G. Uzer, S. Pongkitwitoon, M. Ete Chan and S. Judex, *J. Biomech.*, 2013, **46**, 2296–2302.
64 S. Wang, Y. Liu, Y. Tang, W. Zhao, J. Li, Y. Yang, W. Du and H. Yu, *Clin. Implant Dent. Relat. Res.*, 2014, DOI: 10.1111/cid.12220.
65 G. Uzer, W. R. Thompson, B. Sen, Z. Xie, S. S. Yen, S. Miller, G. Bas, M. Styner, C. T. Rubin, S. Judex, K. Burridge and J. Rubin, *Stem Cells*, 2015, **33**, 2063–2076.
66 B. Sen, Z. Xie, N. Case, M. Styner, C. T. Rubin and J. Rubin, *J. Biomech.*, 2011, **44**, 593–599.